Molecular Simulation of Ionic Polyimides and Composites with Ionic Liquids as Gas Separation Membranes

Asghar Abedini, Ellis Crabtree, Jason E. Bara, and C. Heath Turner*

Department of Chemical and Biological Engineering, The University of Alabama,

Box 870203, Tuscaloosa, Alabama 35487, USA

Abstract

Polyimides are at the forefront of advanced membrane materials for CO₂ capture and gas purification processes. Recently, "ionic polyimides" (IPims) have been reported as a new class of condensation polymers which combine structural components of both ionic liquids (ILs) and polyimides through covalent linkages. In this study, we report CO₂ and CH₄ adsorption and structural analyses of an IPim and an IPim + IL composite containing [C₄mim][Tf₂N]. The combination of molecular dynamics (MD) and grand canonical Monte Carlo (GCMC) simulations are used to compute the gas solubility and the adsorption performance with respect to the density, fractional free volume (FFV), and surface area of the materials. Our results highlight the polymer relaxation process, and its correlation to the gas solubility. In particular, the surface area can provide meaningful guidance with respect to the gas solubility, and it tends to be a more sensitive indicator of the adsorption behavior versus only considering the system density and FFV. For instance, as the polymer continues to relax, the density, FFV, and pore-size distribution remain constant, while the surface area can continue to increase, enabling more adsorption. Structural analyses are also conducted to identify the nature of the gas adsorption once the ionic liquid is added to the polymer. The presence of the IL significantly displaces the CO₂ molecules from the ligand nitrogen sites in the neat IPim to the imidazolium rings in the IPim + IL composite. Whereas, the CH₄ molecules move from the imidazolium ring sites in the neat IPim to the ligand nitrogen atoms in the IPim + IL composite. These molecular details can provide critical information for the experimental design of highly selective IPim materials, as well as provide additional guidance for the interpretation of the simulated adsorption systems.

1. Introduction

Industrial gas separation and storage processes present many technical and economic challenges to the natural gas industry and to power plants. For instance, the existence of acid gases such as H₂S and CO₂ in natural gas increases equipment maintenance and separation cost for the energy industry. To make energy supply lines more economically feasible and minimize corrosion, these impurities must be removed through natural gas sweetening with removal of CO₂ prior to routing natural gas to the supply line. Furthermore, CO₂ is the primary waste component of power plant exhaust gas and is a side product of many processes of the petrochemical industry, such as ammonia production. Palliating CO₂ from emission sources is a critical need in industry, and it is necessary in order to meet current and future environmental regulations. Aqueous alkanolamine (e.g., monoethanolamine (MEA)) solvents are the most common process liquids for CO₂ absorption units. However, these current separation processes are challenged by high energy demands for recovery, volatility, corrosivity, and degradation to toxic products.

Adsorption in porous materials is an alternative, energy-efficient method for removing CO₂ from natural gas streams, and the development of materials possessing both high CO₂ selectivity and adsorption capacity are key factors. While CO₂ removal with MEA involves chemisorption (requiring significant regeneration energy), physisorption in porous materials minimizes the regeneration costs. There are some traditional adsorbents that have been widely studied such as activated carbon,^{6,7} zeolites,⁸ metal organic frameworks

(MOFs),^{9,10} and silica gel.¹¹ While these materials provide high surface areas and adsorption capacity, in practical gas separation applications, there can be limits in terms of either their stability, selectivity, or cost.

Polymer materials such polyimides and polymers of intrinsic microporosity (PIMs) are emerging materials that can be used as gas separation membranes which exhibit both high CO₂ permeability (i.e., flux) and selectivity. 12 As opposed to bulk adsorbents, membranes are more amenable to continuous processing, as they achieve separation of CO₂ through the solution-diffusion mechanism. The fractional free volume (FFV) of advanced polyimides and PIMs comes from their rigid, yet contorted molecular structures, ^{13,14} which creates voids and microstructure due to poor packing between polymer chains. 15-19 Unlike MOFs, which are generally crystalline, polyimides and PIMs are glassy amorphous solids and they tend to have much higher stability in aqueous environments. A major advantage of polyimides and PIMs is the ability select/synthesize requisite monomers as a means of tailoring the polymer repeat unit to maximize specific adsorbent/adsorbate interactions. ^{20,21} In order to tailor the selectivity of these materials, we are exploring the behavior of composite structures composed of an IPim matrix to which additional IL has been added. The intent is to leverage the microporous structure of the IPim with the tunability of the IL selectivity. Otherwise, a pure IL solvent typically suffers from high transport resistance and low free volume.²²

Ionic liquids, generally defined as organic salts with melting point temperatures < 100 °C, are potential solvents for gas separation processes.²³⁻²⁵ They have demonstrated high selectivity for CO₂²⁶⁻²⁸ versus CH₄,^{25,29} and this makes ILs promising for applications in natural gas sweetening and pre-combustion CO₂ capture. In addition, the energy required

for solvent recovery in ILs can be reduced due to the physical absorption mechanism. Nevertheless, using ILs for gas separation processes has several drawbacks. For instance, the current industrial solvent for CO₂ adsorption, MEA, is at least twenty times less expensive on a per volume basis than even the lowest cost ILs. The second, and possibly the most important drawback for ILs is their high viscosity relative to organic solvents. However, using ILs in membrane systems has significant advantages relative to their use as bulk absorbents.³⁰ The high viscosity of ILs can be mitigated in membrane units, due to the short diffusion paths.³⁰ In addition, the physical stability and processability of IPims make these materials an excellent matrix in which to immobilize ILs.³¹ In a recent publication,³² these hybrid materials have demonstrated excellent CO₂/CH₄ separation performance (ScO₂/CH₄ = 13.1) with enhanced permeability (up to 2242% for CO₂ and 2732% for CH₄) when the IL was present within the ionic polyimide.

Several others have recently examined the properties of PIMs and similar materials for gas separations.³³⁻³⁵ Hart, et al. used molecular simulations to model the CO₂/CH₄ separation performance of nitrogen-containing PIMs (tetrafluoroteraphthalonitrile) and sulfonyl-based PIMs.²⁰ They also evaluated the permselectivity of these membranes for CO₂/CH₄ and CO₂/N₂ separation processes,¹⁵ concluding that the polar sulfonyl functionality increases the gas solubility and permselectivity. With regards to CO₂/CH₄ gas separation, the solubility and permeability of CO₂ increases by adding dipolar functionalities and bulky spirocenter groups on the PIM, since these groups increase both the enthalpy of CO₂ adsorption and FFV. In related work, Calero et al.³⁶ investigated the CO₂ adsorption isotherm and selectivity of CO₂/CH₄ in both a hydrated structure of a covalent organic framework (COF) and in a COF structure with a small amount of IL.

Adding the IL in the COF structure increased the selectivity of the CO₂ without a drastic reduction in the adsorption capacity. In the hydrated COF structure, the adsorption capacity tends to decrease while the selectivity increases in favor of the CO₂. In comparison, PIMs possess an amorphous structure, while the COFs have crystalline structures (more similar to MOFs), but with covalently bonded structures of light elements (C, H, N, O, B, etc.) instead of coordinated metallic ions during the reaction. Covalent bonds of light elements (H, B, C, N, and O) compose the crystal structure in COFs while crystal structures of MOFs are coordinated by metal ions.

While the experimental realization of the first generation of IPim + IL composite materials have already been reported,³² molecular simulations can provide detailed insight into the molecular-level structures and interactions in these systems responsible for the experimentally observed behavior. In our study, the 1-butyl-3-methylimidazolium bis(trifluoromethylsulfonyl)imide ([C4mim][Tf2N]) IL has been chosen to reside within the ionic polyimide matrix because of the structural consistency between the IPim and [C4mim⁺][Tf2N⁻] and because this particular IL has been thoroughly studied and its absorption properties toward CO₂ are well-known (Figure S-2).^{1,37-41} We thoroughly characterize the neat IPim relative to the IPim + IL composite materials by analyzing their average pore size distributions, surface areas, FFV, as well as their adsorption of CO₂ and CH₄. The adsorption data is benchmarked against recent experimental results, and we are able to achieve good agreement with the experimental data,³² but this is only obtained after a moderate densification of the simulation cell. Overall, our study highlights the nuances of structural relaxation and its importance on the emergent adsorption behavior in IPim-

based materials, as well as the changes in the molecular-level adsorption behavior induced by the presence of the IL within the IPim matrix.

2. Simulation Details

Our simulation procedure is comprised of several different steps. First, electronic structure calculations are used to assign partial charges on the atom sites of the IPim monomer units. Then, molecular dynamics simulations (MD) are used to prepare the relaxed initial structure of the neat IPim and IPim + IL composite, and this involves a polymerization scheme, followed by several stages of structural relaxation. The initial system also contains an N-methyl-2-pyrrolidone (NMP) solvent, which is eventually removed and replaced with the IL species following polymerization, and this is intended to mimic the experimental synthesis procedure.³² Finally, using an iterative combination of molecular dynamics and grand canonical Monte Carlo (GCMC) simulations, the solubility of CO₂ and CH₄ is modeled over a wide range of different pressures within the neat IPim and IPim + IL composite materials. The details of each stage are described below, and a schematic overview of our simulation models is illustrated in Figure 1.

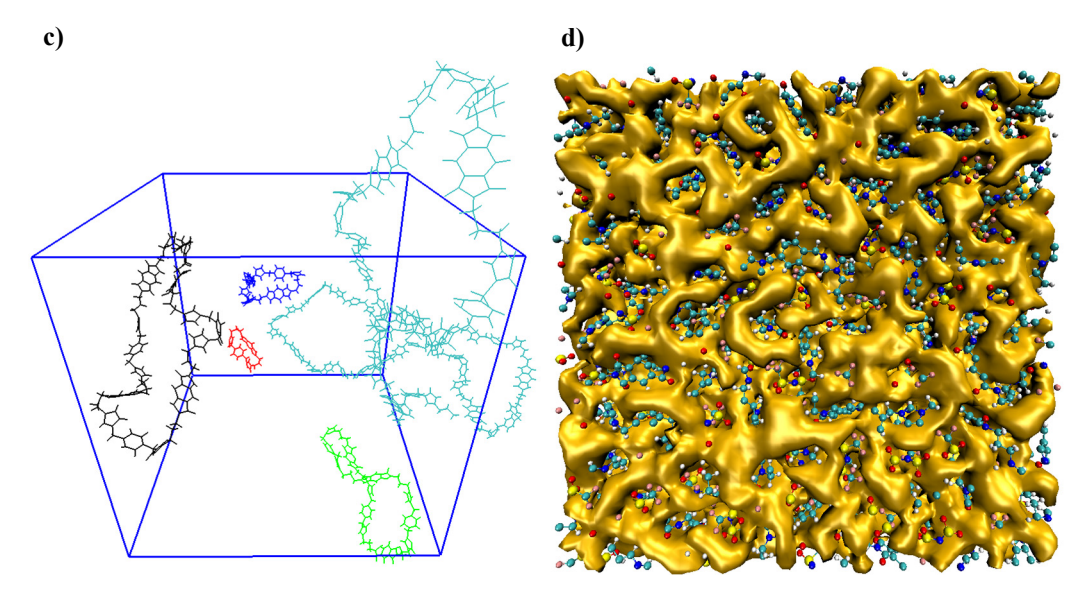


Figure 1. Representative overview of the simulation models: a) IPim monomer, atoms are colored according to their type (N = navy, O = red, C = grey, and H = white). Specific nitrogen sites of the IPim are labeled for reference, as well as the head (H) and tail (T) designation; b) 2-dimensional monomer representation; c) post-polymerization with different chain lengths (red: 1, blue: 2, green: 3, black: 4, and cyan: 12 monomers). $[Tf_2N^-]$ and NMP are deleted for clarity; and d) visualization of the FFV (gold region) within the final polymer system.

In the electronic structure calculations, the geometric optimization of the isolated monomer structure was conducted using the B3LYP functional⁴² with the 6-31G(d) basis set using Gaussian09.⁴³ Using the relaxed structure, the partial charges on each atom were approximated using the ChelpG method.⁴³ Other charge assignment schemes (Hirschfeld, NBO, Merz-Kollman) were also evaluated, and consistent results were found. Ultimately, the partial charge results from the ChelpG method were used to modify the monomer topology file in combination with OPLS-AA force field parameters for monomer interactions. Force field parameters for [C4mim][Tf2N] ILs were taken from Lopez, et al,^{44,45} while parameters for NMP molecules were extracted from Aparicio, et al.⁴⁶ The TraPPE⁴⁷ force field for CO₂, and CH₄ was used, based on the previous experience of others modeling gas adsorption in ILs.^{1,27,48} The Lorentz-Berthelot mixing rules were used for cross-term interactions.

Following the assignment of the force fields, the IPim and IPim + IL systems were constructed and conditioned according to the following default procedure (with specific variations noted later in the text):

- a) Ionic polyimide monomers were inserted into the simulation box using PACKMOL,⁴⁹ followed by energy minimization using the steepest descent algorithm. In order to test for finite-size effects, systems with 55, 110, and 200 monomer units were tested (along with the balance of [Tf₂N⁻] molecules to maintain charge neutrality). In addition, each of these systems was run at least twice, in order to evaluate the reproducibility of the results.
- b) In addition to the monomers, NMP molecules were also inserted at three different ratios: 1:4, 1:6, and 1:8 (monomer:NMP). The experiments used a ratio of approximately 1:60 during polymerization.³²
- c) The monomer + NMP molecules were relaxed with MD simulations using a cycle of canonical (NVT) to increase the temperature following with isothermal-isobaric (NPT) ensemble simulations at high temperature and pressure, followed by a slow quench to room temperature.
- d) The monomer units were polymerized, using a nearest-neighbor algorithm (described below), followed by additional relaxation with MD.
- e) The NMP was then removed from the system, and the IPim + IL samples were generated by inserting the IL molecules in the cavities left by the NMP molecules, again using PACKMOL.

f) Both neat IPim and IPim + IL systems were further equilibrated and relaxed via NVT and NPT cycles, until a final temperature of 294 K and a pressure of 1 bar was reached.

All of the MD simulations were performed with the GROMACS 5.0 simulation package.⁵⁰ The Lennard-Jones potential and electrostatic interactions were calculated with a cut off distance of 1.4 nm, and the smooth particle mesh Ewald sum (SPME)⁵¹ method was implemented for long-range electrostatic interaction with 0.16 nm of Fourier-spacing. The Nose-Hoover thermostat⁵² was used to maintain the temperature and the Parrinello-Rahman⁵³ barostat was used to maintain the pressure, and the time step was 1 fs. In the MD simulations, periodic boundary conditions were implemented in all three dimensions.

In order to test for finite-size effects and to evaluate system equilibration, the configurations of the initial monomer systems were compared with respect to different system sizes (55, 110, and 200 monomers, which correspond to box lengths of approximately 4, 5, and 6 nm, respectively) and different simulation durations. In order to help analyze the initial structural relaxation of the monomers, radial distribution functions (RDFs) were calculated for the tail (T) and head (H) carbons of the monomers, as labeled in **Figure 1**. The RDF results are shown in **Figure S-1**, indicating that at short times (~10 ns) there are some slight inconsistencies in the system configurations between different independent runs with varying box sizes, but at longer time (~50 ns), there is excellent agreement among the 3 different system sizes. Also, after this relaxation and decreasing the temperature to 294 K, the density is very consistent for all boxes (1.614 g/cm³) at the final pressure of 1 bar.

After the monomer relaxation, polymerization was then performed by connecting the head and tail groups, according to a nearest-neighbor algorithm. More sophisticated approaches have also been used to emulate the polymerization process, such as the *Polymatic* algorithm,⁵⁴ which temporarily assigns charges to the head and tail groups of the monomers (accelerating the pairing process). Karayiannis, et al.⁵⁵ suggested that low-density polymerization helps to provide free volume for sufficient mobility and flexibility of the chain. Thus, our polymerization step was conducted at an elevated temperature of 550 K and a pressure of 1 bar, in order to provide for effective conformational flexibility. The monomers were attached using an in-house code that analyzed the H-to-T separation distance, and if within a cutoff (1.27 nm on average), then a hydrogen atom from each head and tail is removed, followed by the formation of a covalent bond.

The prepared IPim structures then followed a steepest-descent energy minimization step for all bonded and non-bonded interactions.⁵⁶ In past work, it has been noted⁵⁵ that temperatures as high as 2000 K were needed to achieve adequate fluctuation and relaxation of glassy polymers. Thus, after polymerization, we continued the equilibration process at a temperature of 2000 K in both the NVT and NPT ensembles prior to cooling to the desired temperature of 294 K. With different initial box sizes (4, 5, and 6 nm) and different initial monomer configurations, the final polymer length distributions varied somewhat. In order to estimate the reproducibility of our results, these different replicas were all evaluated in our physical and adsorption property analysis. A summary of the different IPim systems is described in Table 1.

Table 1. Summary of different IPim systems simulated, with densities corresponding to conditions of 1 bar and 294 K.

description (including approximate box length)	# monomers	# NMP	density (g/cm ³)	polymer chain lengths*
neat, 4 nm (sample 1)	55	0	1.602	29, 10, 7, 7, 2
neat, 4 nm (sample 2)	55	0	1.602	42, 9, 2, 2
neat, 5 nm (sample 1)	110	0	1.625	78, 10, 17, 5
neat, 5 nm (sample 2)	110	0	1.604	33, 46, 2, 14, 15
neat, 6 nm (sample 1)	200	0	1.601	15, 20, 76, 56, 29, 2, 2
neat, 6 nm (sample 2)	200	0	1.641	17, 8, 8, 5, 5, 4(6), 3(11), 2(18), 1(64)
neat, 6 nm (sample 3)	200	800	1.600	80, 13, 41, 40, 20, 6
composite, 6.8 nm (sample 1)	200 (+ 200 IL)	800	1.580	80, 13, 41, 40, 20, 6
composite, 6.8 nm (sample 2)	200 (+ 200 IL)	1200	1.584	178, 14, 8

^{*}Numbers inside the parentheses represent the replication of that polymer chain length.

As mentioned previously, the experimental production of the IPim samples involved the addition of NMP (5 mL per gram of monomer, which is a monomer:NMP molar ratio of 1:60).³² After the experimental polymerization reaction is complete, the side products and solvents are removed from the polymer. In order to mimic this process and to create the temporary voids for the IL insertions, the NMP molecules were present throughout the monomer equilibration and polymerization steps. After system equilibration and polymerization, the NMP molecules were then deleted from the box and the void spaces filled with [C4mim][Tf2N] molecules using PACKMOL software. To make sure that we made enough space for [C4mim][Tf2N] and were able to generate a well-mixed system, we started with three different ratios of monomer:NMP molecules of 1:4, 1:6, and 1:8. For consistency with the experiments, the IL was added to the IPim at the same concentrations of 50:50.

Once the neat IPim ionic polyimide and IPim + IL samples were prepared, we used the Cassandra package to run grand canonical Monte Carlo (GCMC) simulations of CO₂

and CH₄ adsorption.⁵⁷ During GCMC simulations, the polymer and IL molecules are held rigid, while the GCMC steps involving the gas adsorbates were run for at least 3 × 10⁶ steps (with 33% insertion, 33% deletion, 17% translation, and 17% rotation). In order to improve sampling, these GCMC simulations were iteratively combined with MD simulations to further relax the system configuration. For instance, after finishing one stage of GCMC simulations, the resulting structure (including the gas molecules) was subjected to a short NVT MD relaxation process of 1 ns at the same temperature (294 K). After the MD stage, the resulting structure was then transferred back to the GCMC stage for continued insertion and deletion of gas molecules. This process continued for at least three cycles for each point along the adsorption isotherm, and the average value of the final GCMC cycles is reported in the isotherm graphs and also used to calculate Henry's constants. Henry's constant was extracted from the slope of the fitted line to the solubility graph, which was then converted from units of g/(L·bar) to mol/(L·atm).

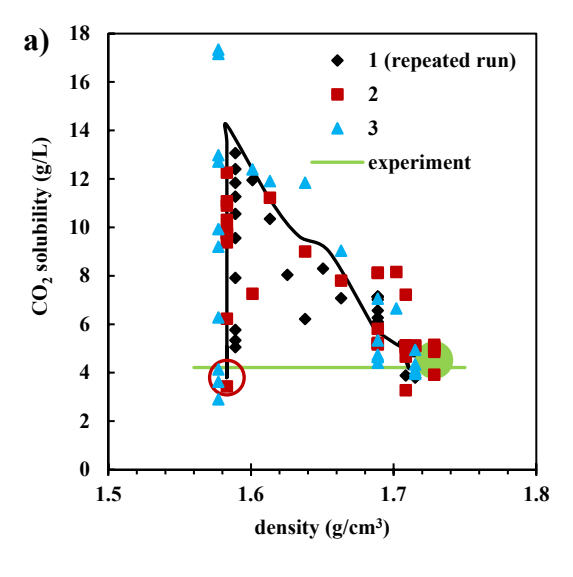
In order to connect the IPim and IPim + IL composite adsorption properties to the underlying molecular configurations, several different structural analyses were performed, which were originally applied to characterize solid adsorbents. Using the approaches of Gelb and Gubbins,⁵⁸ we calculate the fractional free volume (FFV), pore size distribution (PSD), and exposed surface area of our IPim and IPim + IL composite models (which include all atomic sites during the analysis, with the Lennard-Jones diameters used to define the molecular surfaces), as well as the radial distribution function of key interaction sites in the system.

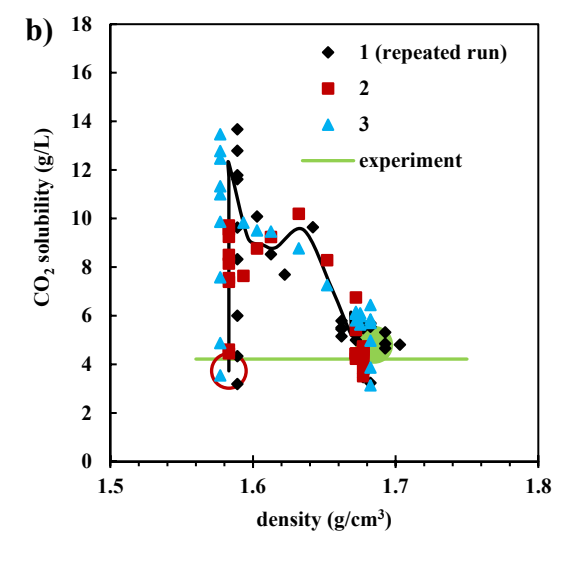
3. Results and Discussion

3.1. Structural Optimization

The densities of the neat IPim and IPim + IL composite systems were optimized, in order to reproduce the experimental CO₂ adsorption data. Thus, the initial system densities $(\sim 1.6 \text{ g/cm}^3)$ were slightly decreased to $1.565 \sim 1.589 \text{ g/cm}^3$, while the adsorption behavior was predicted by the GCMC simulations (with the IPim and IPim + IL composite considered rigid). These simulation results are indicated by the large red circles in Figure 2, and they compare well with the experimental data. From these initial simulations, the IPim and IPim + IL composite structures were further subjected to stages of MD relaxation. Even though the systems were thoroughly relaxed prior to the initial GCMC simulations, the presence of the adsorbate molecules tends to help condition the adsorbent to increase its capacity. Each MD stage tends to further relax the system, providing additional adsorption capacity during the subsequent GCMC stage. Thus, at a fixed system density, the adsorption still continues to increase by a factor of 2-3 by subjecting the system to additional MD/GCMC stages. Thus, in order to capture the experimental behavior, the system was then gradually compressed until the adsorption approached the experimental values. The optimized IPim structures had densities approximately 10% higher (1.72 \pm 0.03 g/cm³) after the compression steps, with the final values indicated by the green circles in Figure 2. Each system optimization was repeated three times from the initial structure to the optimized one to evaluate the reproducibility of the results. All GCMC simulations were performed at 294 K and 1 bar for $3\sim5\times10^6$ MC steps while MD calculations were implemented in the NVT ensemble for 1 ns at 294 K. These final structures were used to calculate the gas adsorption isotherms, as well as for the structural analyses. We followed the same procedure to optimize the IPim + IL composite, leading to a final density of 1.62 \pm 0.02 g/cm³.

In the experiments, an NMP solvent was used during the initial polymerization,³² and then washed away prior to adsorption. To consider the effect of NMP on the simulated structure and gas solubility results, we compared two samples: one includes NMP during polymerization and one is conducted without NMP molecules during polymerization (**Figure S-3**). After polymerization, the NMP molecules were deleted from the system, followed by relaxation of both systems. As **Figure S-3** shows, the presence of the NMP solvent during the polymerization simulations does not appreciably affect the final gas solubility. The sample without NMP is referred to as "neat, 6 nm (sample 1)" and the sample with NMP is referred to as "neat, 6 nm (sample 3)". Although they show a noticeable difference in the first GCMC simulations, their gas adsorption properties converge very closely after 4 cycles of MD/GCMC. Thus, the temporary presence of the NMP molecules was useful for preparing the IPim+ IL composites, but the NMP does not seem to be responsible for any other residual effects on the gas adsorption performance.





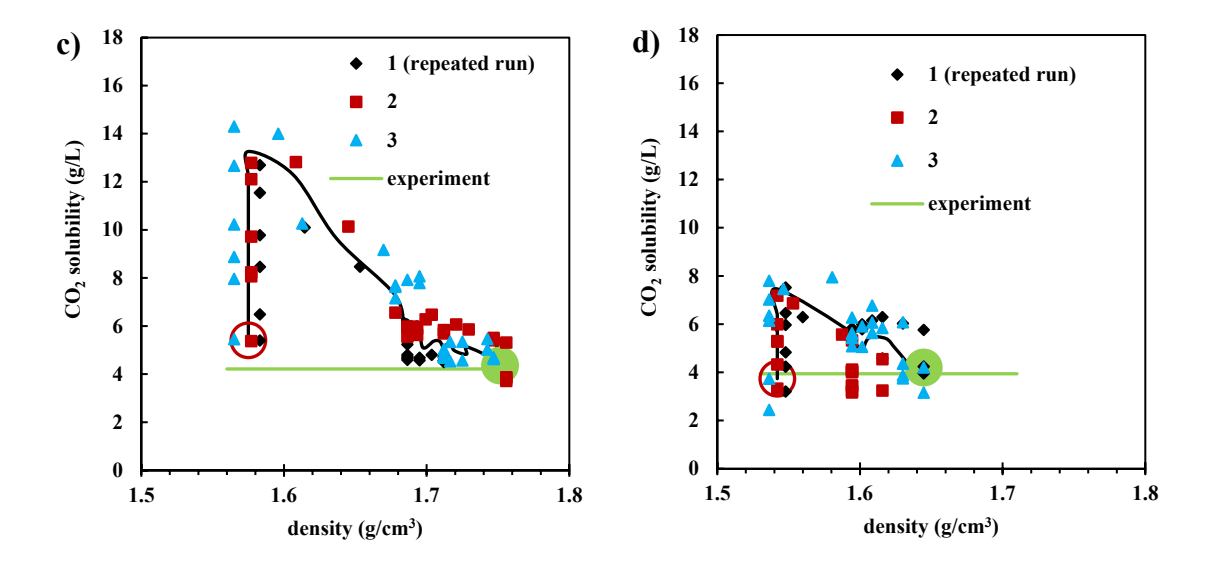


Figure 2. CO₂ solubility during densification and relaxation for: a) 55 monomers; b) 110 monomers; c) 200 monomers; and d) 200 monomers in 200 [C₄mim][Tf₂N]. These results are extracted from incremental cycles of MD and GCMC simulations, with each point corresponding to one MD/GCMC cycle. The hollow red circle is the starting point, the green circle is the final optimized structure, and the solid black line is a guide to the eye corresponding to successive cycles. The green line represent the experimental data,³² with a standard deviation of < 5%.

3.2. Structural Analysis

As illustrated in the previous section, the polymer adsorbent shows different solubility values at constant density. While switching back and forth between MD and GCMC calculations, the polymer structure was increasingly relaxed to accept more CO₂ molecules. In order to make the connection between the adsorption data and the different simulation structures, the surface area and FFV were calculated at different points along the simulation trajectory. During the MD simulations, the polymer molecules were free to modify their positions, and during GCMC calculation this modification helped the structure accept more gas molecules until the structure was saturated at the desired temperature and pressure. The exposed surface area (calculated as an average over multiple independent configurations at each stage) can help characterize the structural modification from the initial point to the maximum point of the solid line. At constant density, from the red hollow circle to the

maximum point of the solid line, the surface area in the polymer structure increased (**Figure 3**), while the FFV is constant (**Figure 4**). As **Figures 3 and 4** show, the predicted solubility tends to be much more sensitive to the exposed surface area versus the FFV, which is typically used as a surrogate to predict gas solubility.

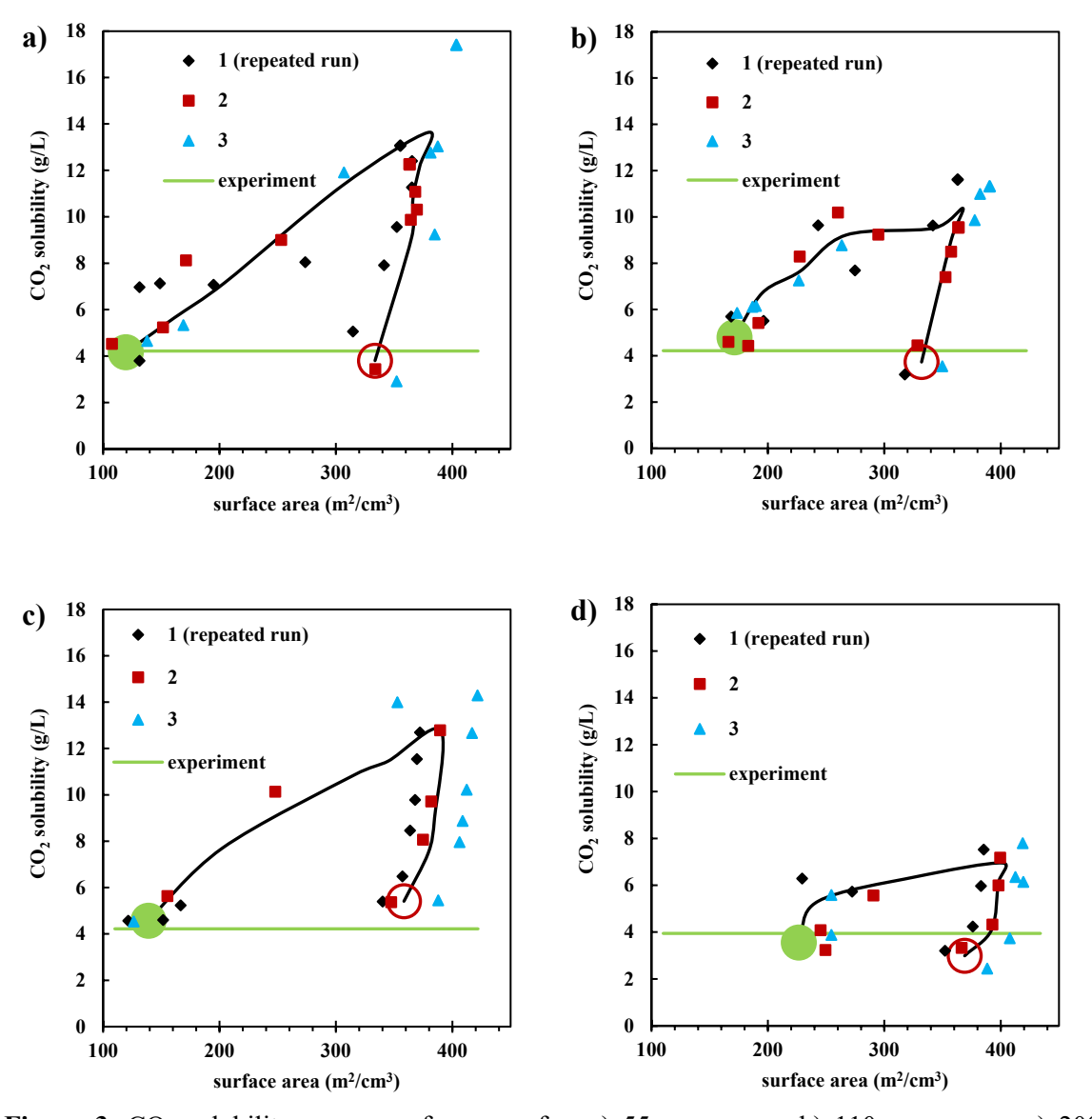


Figure 3. CO₂ solubility versus surface area for: a) 55 monomers; b) 110 monomers; c) 200 monomers; and d) 200 monomers in 200 [C₄mim⁺][Tf₂N⁻]. The results are extracted from successive cycles of MD/GCMC simulations. The hollow red circle is the starting point, the green circle is the optimized structure, and the black solid line is a guide to the eye.

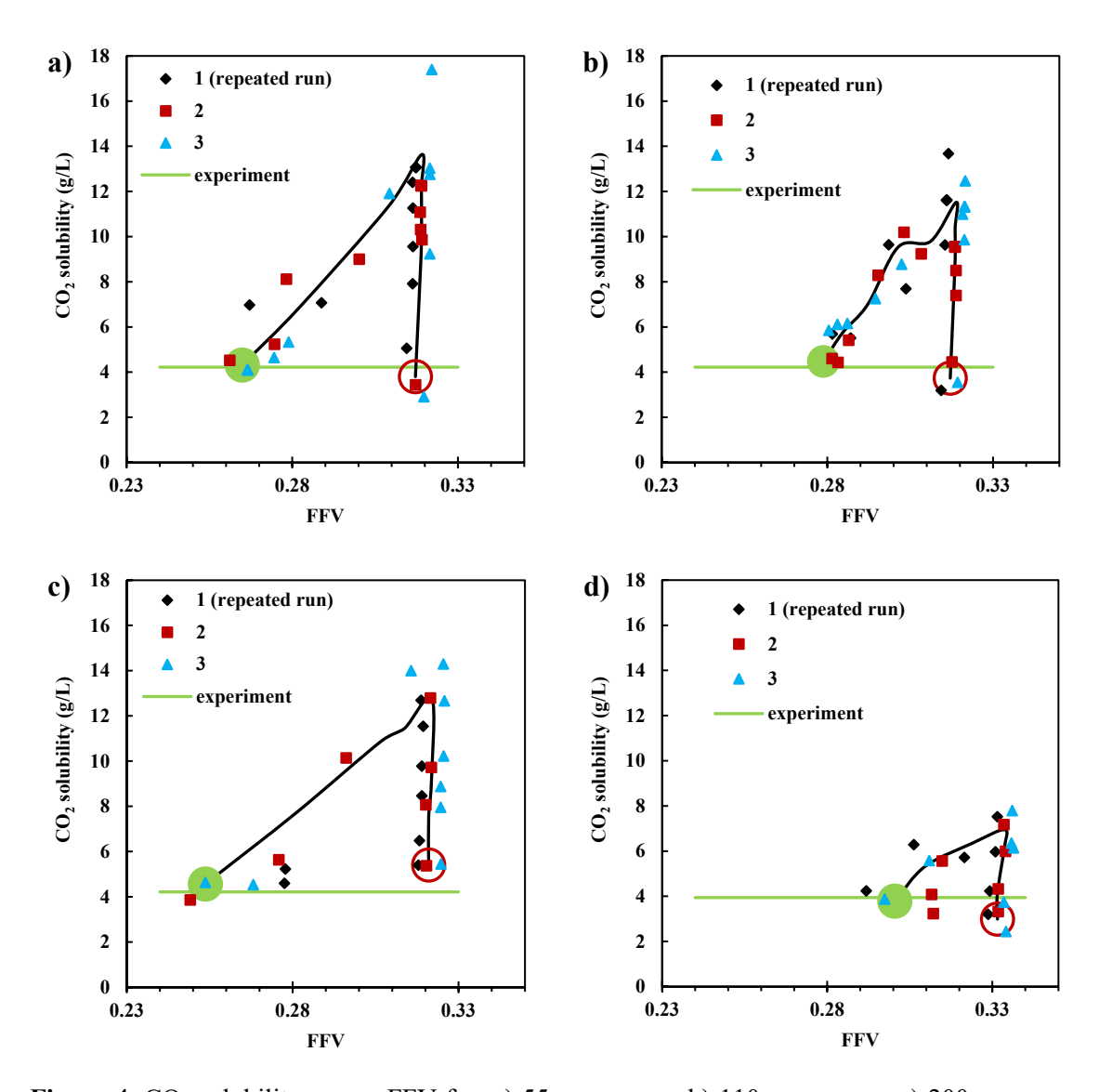


Figure 4. CO₂ solubility versus FFV for: a) 55 monomers; b) 110 monomers; c) 200 monomers; and d) 200 monomers in 200 [C₄mim][Tf₂N]. The results are extracted from successive cycles of MD/GCMC simulations. The hollow red circle is the starting point, the green circle is the optimized structure, and the black solid line is a guide to the eye.

The pore size distribution is one of the key factors for characterizing the gas separation properties of porous materials. **Figure 5** shows the pore size distribution of our IPim systems at 294 K (corresponding to both initial and final structures). The solid lines represent the initial structures (densities of 1.565 ~ 1.589 g/cm³), while the dashed lines represent the final optimized structures. As the density increases, the PSD shifts towards

smaller pore sizes, and the FFV decreases, as well. The smaller pore sizes reduce the adsorption capacity of the polymer for both CO₂ and CH₄. **Figure 5** shows that similar densities tend to possess similar FFVs and similar pore size distributions. However, as noted previously, the calculated surface area can provide additional distinction between these systems, and the surface area calculation can be performed very efficiently (significantly faster than calculating the PSD).

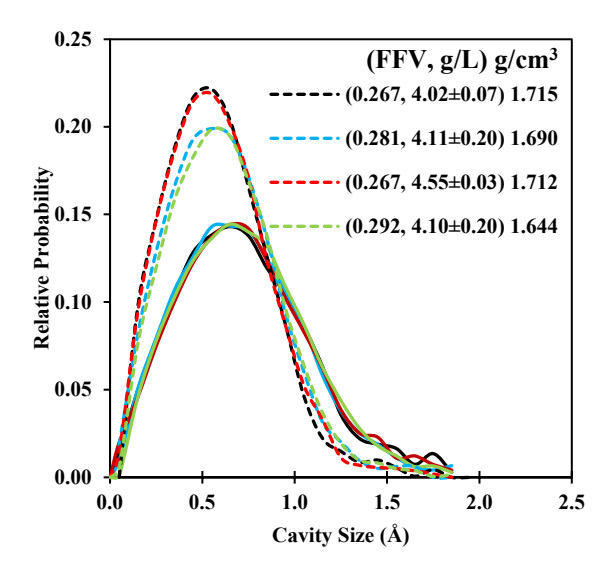


Figure 5. Pore size distribution of initial structures (solid lines) and optimized, compressed structure (dashed lines) at 294 K. Colors represent different polymer systems: 55 monomers (black), 110 monomers (blue), 200 monomers (red), and 200 monomers + IL (green). Fractional free volume, CO₂ solubility, and the density are reported for the optimized structures.

3.3. Gas Solubility

The partial pressures of CO_2 in exhaust gases of power plants and flare chambers are around atmospheric pressure. Therefore, we have calculated the isotherm of the desired gases (CO_2 and CH_4) over the range of pressures from 1×10^{-3} bar up to atmospheric conditions. The experimental CO_2 and CH_4 solubility³² at atmospheric pressure and 294 K have been used to benchmark our results (**Figure 6**). Adding ILs to the pure polymer did

not significantly change the solubility of the gas in the IPim. However, upon further analysis, we are able to identify very different molecular interactions between the gas molecules and the IPim and IPim + IL systems.

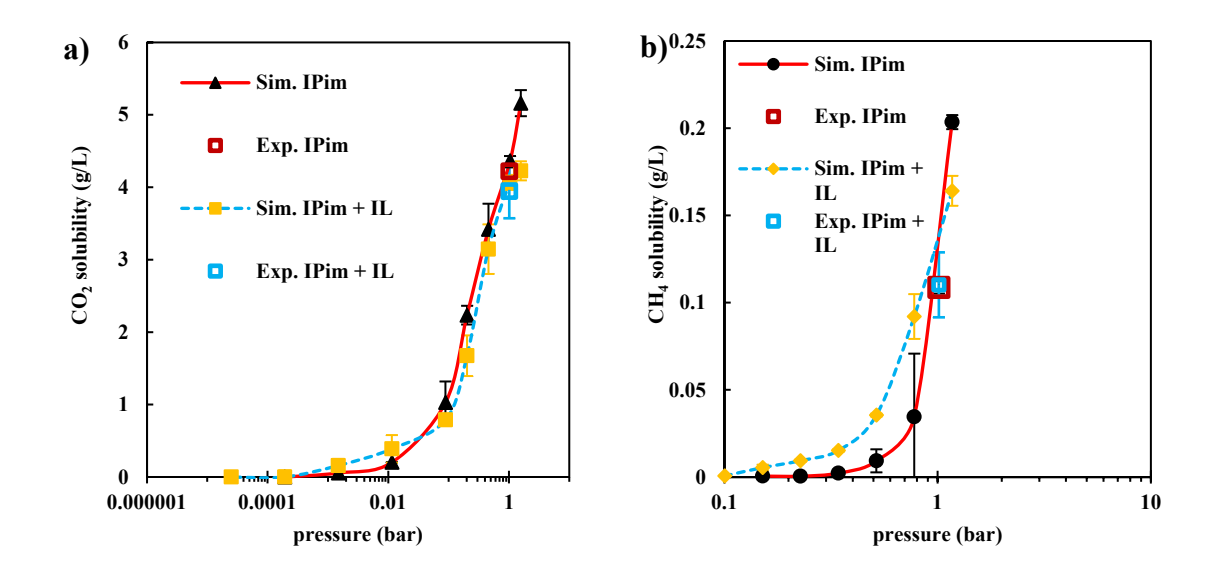


Figure 6. Adsorption isotherms at 294 K of: a) CO₂, b) CH₄ (gas solubility values are provided in **Table S-2**).

The Henry's constant was also calculated for CO₂ and CH₄ in the IPim. Adding the IL to the IPim did not significantly affect CH₄ solubility (0.012 for IPim and 0.009 mol/(L·atm) for IPim+IL). Surprisingly, adding the IL to the IPim slightly reduced the solubility of the CO₂ (0.075 for IPim and 0.066 mol/(L·atm) for IPim+IL composite). The Henry's law constant in this report was calculated at 294 K over a pressure range of 0 to 1 bar. In comparison, the reported experimental Henry's law constant for CO₂ and CH₄ in [C₄mim][Tf₂N] is 0.066 and 0.010 mol/(L·atm), respectively. The experimental Henry's law constant was reported at 333 K over a pressure range of 0 to 5 bar for CO₂ and 0 to 20 bar for CH₄. ^{1,25,59} Additional data for carbon dioxide and methane solubility in 1-ethyl-2-methylimidazole and 1-pentyl-2-methylimidazole is included in **Table S-1**. ⁶⁰ According to

the simulation and experimental results, adding the IL to the polymer (at a ratio of 50:50) did not significantly change the adsorption of the polymer in favor of CO₂. However, the IPim and IPim + IL composite still strongly adsorb CO₂ versus CH₄, and the experiments indicate a significant increase in gas permeability, which we intend to investigate further in future work.

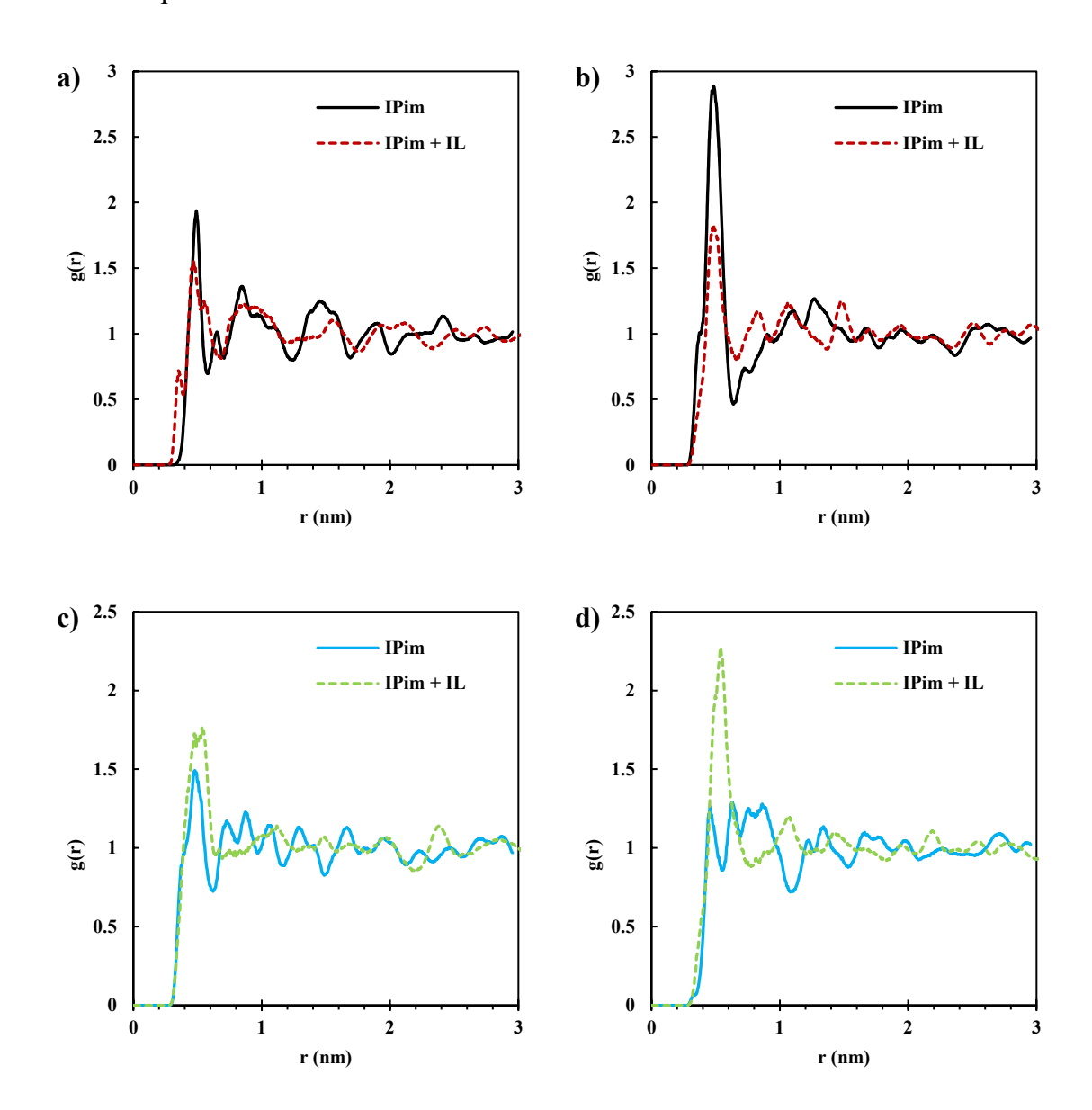
3.4. Analysis of Adsorbate Interactions

Identifying the dominant CO₂ adsorption interactions in our IPim and IPim + IL composite models can reveal useful information for understanding the current gas adsorption behavior and also help guide the design for future IPim-based materials. In particular, it is important to characterize the adsorption site preferences for CO₂ versus CH₄, since it is difficult to anticipate the balance of adsorption enthalpy and site accessibility in our amorphous structures. To help identify the site selectivity for CO₂ and CH₄, we analyzed the RDFs of the gases with specific sites of the IPim. In order to calculate the RDFs, we extracted 10 different configurations at each stage (each separated by $0.5 \times$ 10⁶ steps). Each of these extracted samples was further relaxed with MD simulations for 10 ns, and the reported RDFs are the average of these 10 samples. We have labeled six different nitrogen atoms in the monomer structure: N1 and N2 represent the ligand nitrogen atoms while N3 to N6 represent the imidazolium ring nitrogen atoms in the monomer structure (see Figure 1). As Figure 7 shows, the ligand nitrogen atoms in the IPim have strong interactions with the adsorbed CO₂ gas. After the addition of the IL, this interaction is weakened and the adsorbed CO2 molecules are located mostly around the imidazolium ring of the polymer. Since the polymer structure is fairly symmetric, the adsorbed CO₂ may move to either the right or left side of the ligand. However, as Figure 7 b shows, CO₂ molecules are likely attracted to the N2 atom of the ligand. Thus, it is more probable that CO₂ molecules were moved toward the first imidazolium ring containing N3 and N4. As **Figure 7 c,d** show, the interaction intensity of the adsorbed gas molecules with N3 and N4 is higher in the IPim + IL composite, while the intensity of the CO₂ interactions with N5 and N6 remains unchanged (**Figure 7 e and f**).

Methane shows very different interactions with the adsorbent structures. As **Figure 8** shows, CH₄ molecules are mostly located at N5 and more specifically at N6 sites of the imidazole ring of the polymer. Adding the IL to the IPim changes the preferred CH₄ locations. Composite structures of IPim + IL have strong interactions between the CH₄ and the N1 atom, since it is the closest nitrogen atom to the N6 in the monomer structure (**Figure 8 a**). The interaction strength between the N3 site and CH₄ will increase upon the addition of the IL (**Figure 8 c**). Overall, CO₂ molecules are most likely located at the ligand site of the IPim and adding IL moves them toward the imidazolium ring of the monomer. However, CH₄ molecules are mostly located near the imidazolium ring site of the monomer, and adding the IL to the IPim moves the CH₄ molecules toward the ligand site of the monomer.

This work reports pure gas adsorption simulations. However, competition of CO₂/CH₄ to occupy the active sites of the composite structure in different concentrations of CO₂/CH₄ may reveal more information about the selectivity of this structure. This will be investigated in future work. As **Figures 7 and 8** show, the interaction of the IPim + IL composite with CO₂ is stronger and well distributed along the nitrogen sites of the polymer than its interaction with CH₄. To support this idea, **Figure 9** compares the interaction of CO₂ and CH₄ with [Tf₂N⁻] in the IPim and composite structure. While the CO₂ interaction

remains constant in both structures, the CH₄ interaction with $[Tf_2N^-]$ decreases significantly in the composite structure.



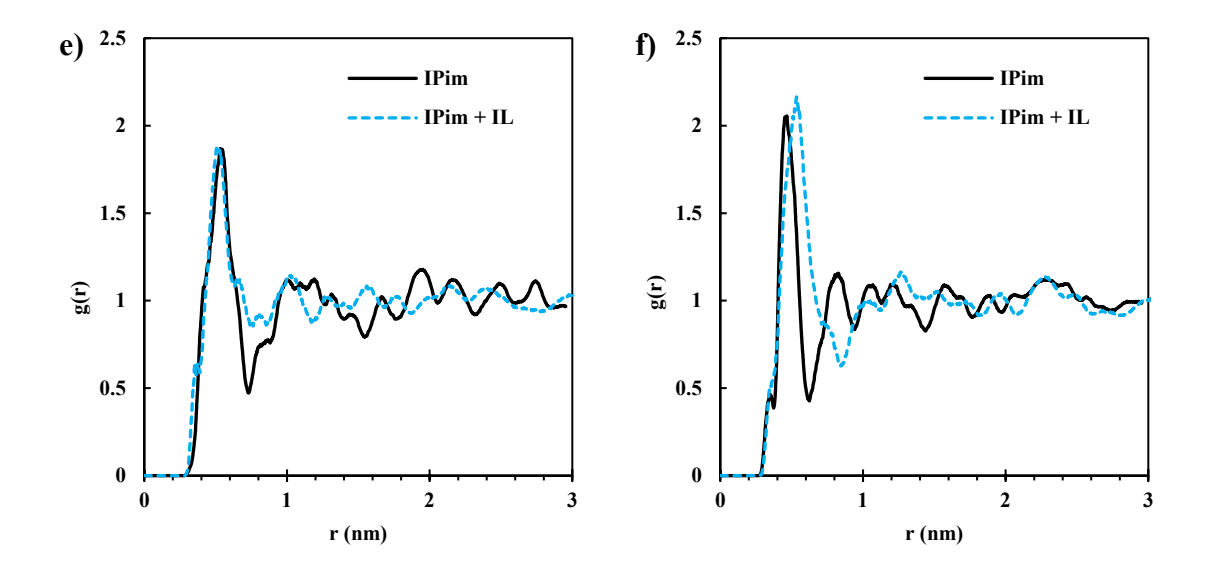
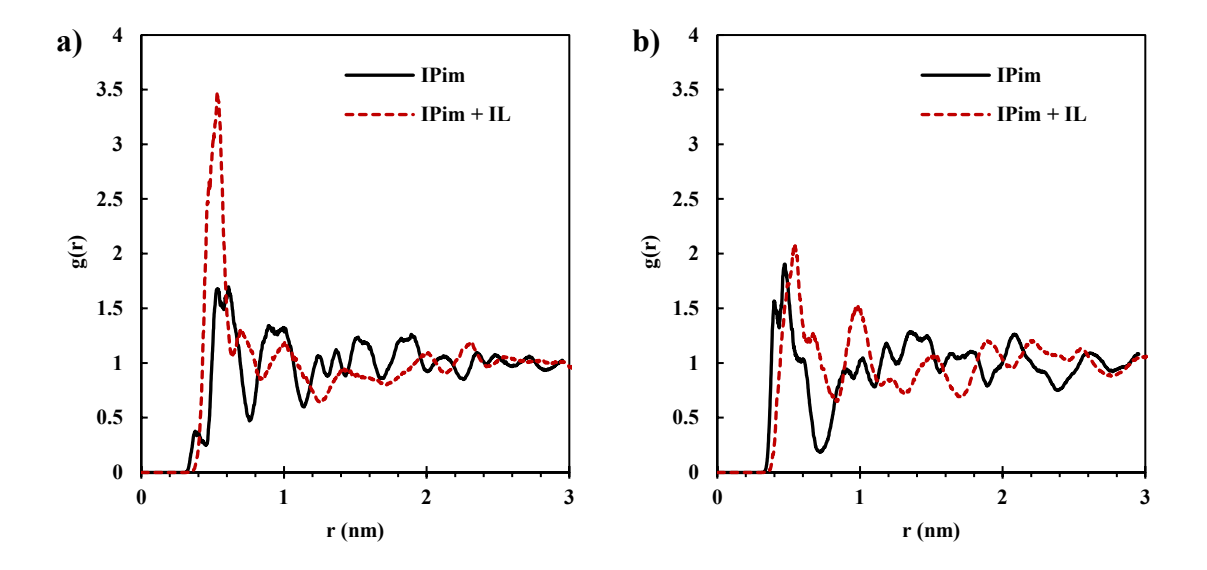


Figure 7. Radial distribution function between the carbon atom of CO₂ and the IPim sites: a) N1; b) N2; c) N3; d) N4; e) N5; and f) N6 (see Figure 1 for site labels).



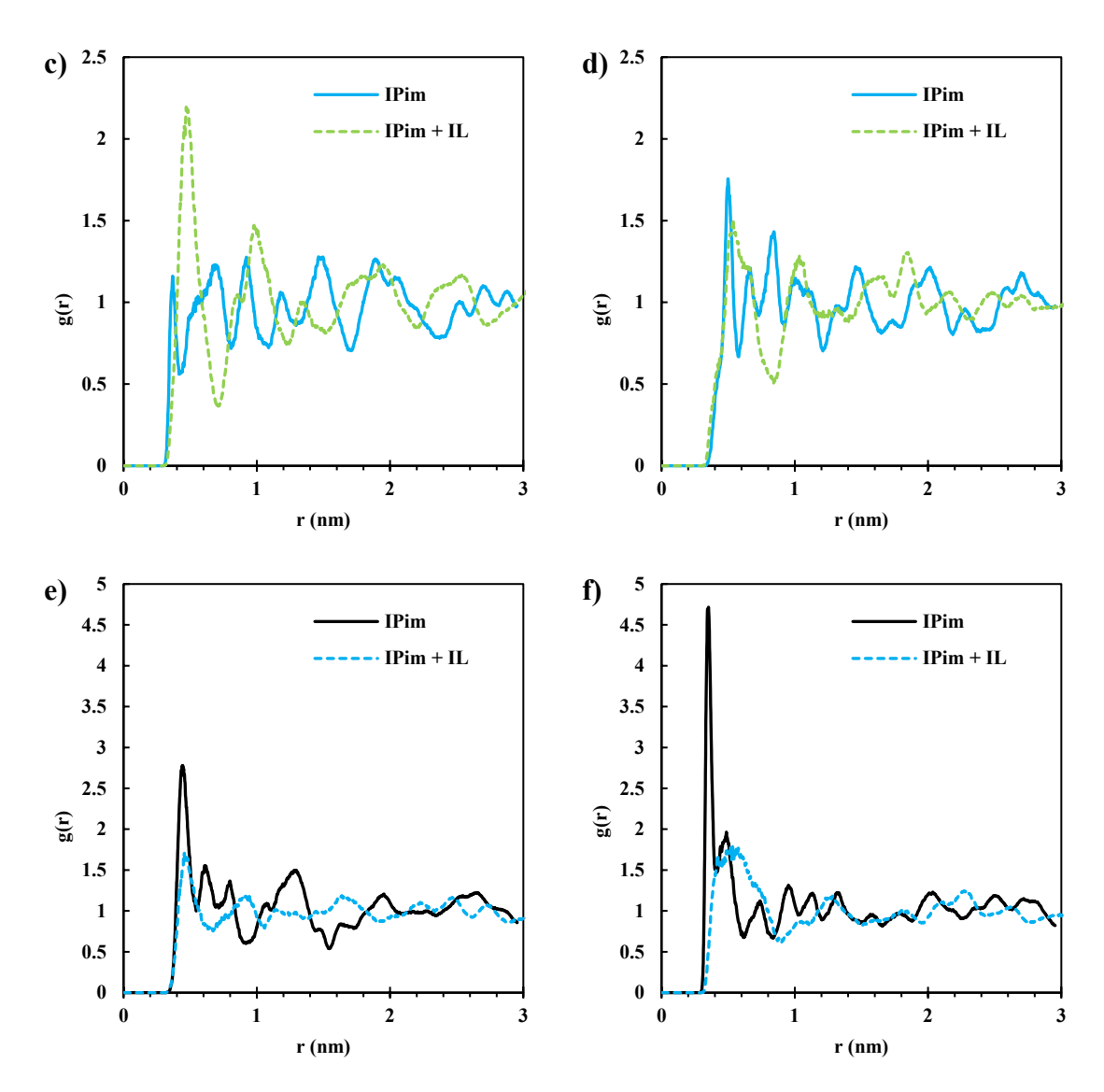


Figure 8. Radial distribution functions of the carbon atom of CH₄ with the IPim sites: a) N1; b) N2; c) N3; d) N4; e) N5; and f) N6 (see Figure 1 for site labels).

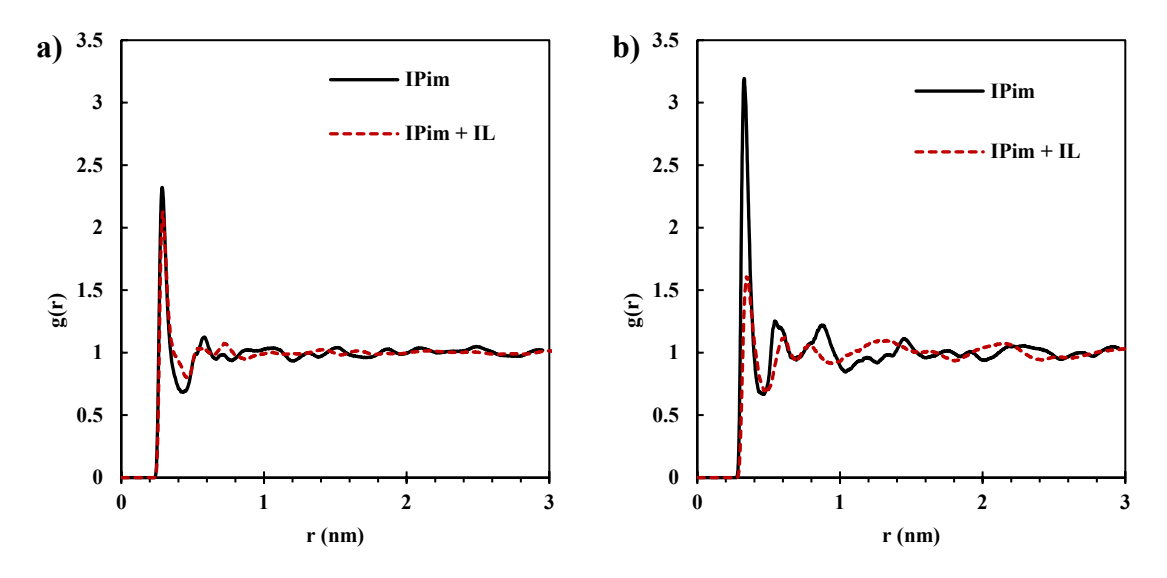


Figure 9. Radial distribution function of the oxygen atoms of the $[Tf_2N^-]$ anions with the carbon atoms of: a) CO_2 ; and b) CH_4 (see Figure 1 for site labels).

4. Conclusion

In this study, the solubility of CO₂ and CH₄ in an IPim and an IPim + [C₄mim][Tf₂N] composite was predicted and benchmarked against experimental values. In addition, the structural details of the adsorbents and the molecular-level interaction with the gas molecules were identified. Several different aspects were highlighted. First, the cyclical relaxation between MD and GCMC was found to have a significant effect on the adsorption capacity. Even though the adsorbents were thoroughly relaxed prior to the initial GCMC stage, further relaxation with MD in the presence of the CO₂ was found to significantly increase the gas adsorption. Second, by tracing the structural relaxation of the system, we found that the exposed surface area of the adsorbent is a fairly sensitive measure of the adsorption performance (while the density, PSD, and FFV remain essentially constant). Finally, although the addition of the IL to the IPim matrix has a negligible effect on the relative adsorption of CO₂ and CH₄, it has a dramatic effect on the nature of the gas adsorption. We predict that the preferred adsorption sites of the CO₂ and CH₄ shift among

the ligand nitrogens and imidazolium nitrogens, depending upon the presence of the IL in the IPim material. Overall, this information is expected to provide important molecular-level details for the design of future IPim and IPim + IL composites for optimizing the transport rates and selectivity of different adsorbates. While the permeability can be significantly enhanced in the IPim + IL compsotiess, specific functionalization of the IPim or IL selection can be used to further increase the selectivity.

In regards to the simulation procedure, a moderate densification of the systems (up to 10%) was required to capture the experimental adsorption data. While this approach may not be transferrable to other systems or to other temperature and pressure conditions, future work will test the generality of such an approach for other IPim and IPim + IL composites. For instance, it is recognized that there are other potential sources for the initial quantitative disagreement with the experiments, such as shortcomings in the intermolecular potential (including the assignment of partial charges). Regardless, we find that a thorough analysis of the system relaxation is necessary, since subtle changes in the system can impart large changes in the predicted adsorption behavior.

Acknowledgements

Support for this work was provided by the National Science Foundation (CBET-1605411) and computer resources were provided by the Alabama Supercomputer Center.

Supporting Information

The Supporting Information is available free of charge on the ACS Publications website at DOI. It includes IPim monomer equilibration analysis, additional illustrations of the molecular models, tests of the influence of the NMP solvent, and Henry's constants.

References:

- (1) Budhathoki, S.; Shah, J. K.; Maginn, E. J. Molecular Simulation Study of the Solubility, Diffusivity and Permselectivity of Pure and Binary Mixtures of CO₂ and CH₄ in the Ionic Liquid 1-n-Butyl-3-methylimidazolium bis(trifluoromethylsulfonyl)imide. *Ind. Eng. Chem. Res.* **2015**, *54*, 8821-8828.
- (2) Aparicio, S.; Atilhan, M. Computational Study of Hexamethylguanidinium Lactate Ionic Liquid: A Candidate for Natural Gas Sweetening. *Energy Fuels* **2010**, *24*, 4989-5001.
- (3) Chang, H.; Shih, C. M. Simulation and optimization for power plant flue gas CO₂ absorption-stripping systems. *Sep. Sci. Technol.* **2005**, *40*, 877-909.
- (4) Liu, Y. D.; Zhang, L. Z.; Watanasiri, S. Representing vapor-liquid equilibrium for an aqueous MEA-CO₂ system using the electrolyte nonrandom-two-liquid model. *Ind. Eng. Chem. Res.* **1999**, *38*, 2080-2090.
- (5) Dupart, M. S.; Bacon, T. R.; Edwards, D. J. Understanding Corrosion in Alkanolamine Gas Treating Plants. *Hydrocarbon Process* **1993**, *72*, 75-80.
- (6) Peng, X.; Wang, W.; Xue, R.; Shen, Z. Adsorption separation of CH₄/CO₂ on mesocarbon microbeads: Experiment and modeling. *AIChE J.* **2006**, *52*, 994-1003.
- (7) Bai, B. C.; Cho, S.; Yu, H.-R.; Yi, K. B.; Kim, K.-D.; Lee, Y.-S. Effects of aminated carbon molecular sieves on breakthrough curve behavior in CO₂/CH₄ separation. *J. Ind. Eng. Chem.* **2013**, *19*, 776-783.
- (8) Heymans, N.; Alban, B.; Moreau, S.; De Weireld, G. Experimental and theoretical study of the adsorption of pure molecules and binary systems containing methane, carbon monoxide, carbon dioxide and nitrogen. Application to the syngas generation. *Chem. Eng. Sci.* **2011**, *66*, 3850-3858.
- (9) García, E. J.; Mowat, J. P. S.; Wright, P. A.; Pérez-Pellitero, J.; Jallut, C.; Pirngruber, G. D. Role of Structure and Chemistry in Controlling Separations of CO₂/CH₄ and CO₂/CH₄/CO Mixtures over Honeycomb MOFs with Coordinatively Unsaturated Metal Sites. *J. Phys. Chem. C* **2012**, *116*, 26636-26648.
- (10) Li, S.; Chung, Y. G.; Snurr, R. Q. High-Throughput Screening of Metal-Organic Frameworks for CO₂ Capture in the Presence of Water. *Langmuir* **2016**, *32*, 10368-10376.
- (11) Morishige, K. Adsorption and Separation of CO₂/CH₄ on Amorphous Silica Molecular Sieve. *J. Phys. Chem. C* **2011**, *115*, 9713-9718.
- (12) Slater, A. G.; Cooper, A. I. Porous materials. Function-led design of new porous materials. *Science* **2015**, *348*, aaa8075-10.

- (13) McKeown, N. B.; Budd, P. M. Polymers of intrinsic microporosity (PIMs): organic materials for membrane separations, heterogeneous catalysis and hydrogen storage. *Chem. Soc. Rev.* **2006**, *35*, 675-683.
- (14) Xiao, Y. C.; Zhang, L. L.; Xu, L.; Chung, T. S. Molecular design of Troger's base-based polymers with intrinsic microporosity for gas separation. *J. Membr. Sci.* **2017**, *521*, 65-72.
- (15) Hart, K. E.; Colina, C. M. Estimating gas permeability and permselectivity of microporous polymers. *J. Membr. Sci.* **2014**, *468*, 259-268.
- (16) Tocci, E.; De Lorenzo, L.; Bernardo, P.; Clarizia, G.; Bazzarelli, F.; McKeown, N. B.; Carta, M.; Malpass-Evans, R.; Friess, K.; Pilnáček, K.; Lanč, M.; Yampolskii, Y. P.; Strarannikova, L.; Shantarovich, V.; Mauri, M.; Jansen, J. C. Molecular Modeling and Gas Permeation Properties of a Polymer of Intrinsic Microporosity Composed of Ethanoanthracene and Tröger's Base Units. *Macromolecules* **2014**, *47*, 7900-7916.
- (17) Swaidan, R.; Ghanem, B.; Litwiller, E.; Pinnau, I. Physical Aging, Plasticization and Their Effects on Gas Permeation in "Rigid" Polymers of Intrinsic Microporosity. *Macromolecules* **2015**, *48*, 6553-6561.
- (18) Heuchel, M.; Fritsch, D.; Budd, P. M.; McKeown, N. B.; Hofmann, D. Atomistic packing model and free volume distribution of a polymer with intrinsic microporosity (PIM-1). *J. Membr. Sci.* **2008**, *318*, 84-99.
- (19) Budd, P.; Msayib, K.; Tattershall, C.; Ghanem, B.; Reynolds, K.; McKeown, N.; Fritsch, D. Gas separation membranes from polymers of intrinsic microporosity. *J. Membr. Sci.* **2005**, *251*, 263-269.
- (20) Hart, K. E.; Abbott, L. J.; McKeown, N. B.; Colina, C. M. Toward Effective CO₂/CH₄ Separations by Sulfur-Containing PIMs via Predictive Molecular Simulations. *Macromolecules* **2013**, *46*, 5371-5380.
- (21) Chen, Y.-R.; Chen, L.-H.; Chang, K.-S.; Chen, T.-H.; Lin, Y.-F.; Tung, K.-L. Structural characteristics and transport behavior of triptycene-based PIMs membranes: A combination study using ab initio calculation and molecular simulations. *J. Membr. Sci.* **2016**, *514*, 114-124.
- (22) Otani, A.; Zhang, Y.; Matsuki, T.; Kamio, E.; Matsuyama, H.; Maginn, E. J. Molecular Design of High CO₂ Reactivity and Low Viscosity Ionic Liquids for CO₂ Separative Facilitated Transport Membranes. *Ind. Eng. Chem. Res.* **2016**, *55*, 2821-2830.
- (23) Anthony, J. L.; Maginn, E. J.; Brennecke, J. F. Solubilities and thermodynamic properties of gases in the ionic liquid 1-n-butyl-3-methylimidazolium hexafluorophosphate. *J. Phys. Chem. B* **2002**, *106*, 7315-7320.

- (24) Kerle, D.; Ludwig, R.; Geiger, A.; Paschek, D. Temperature Dependence of the Solubility of Carbon Dioxide in Imidazolium-Based Ionic Liquids. *J. Phys. Chem. B* **2009**, *113*, 12727-12735.
- (25) Ramdin, M.; Balaji, S. P.; Vicent-Luna, J. M.; Gutiérrez-Sevillano, J. J.; Calero, S.; de Loos, T. W.; Vlugt, T. J. H. Solubility of the Precombustion Gases CO₂, CH₄, CO, H₂, N₂, and H₂S in the Ionic Liquid [bmim][Tf₂N] from Monte Carlo Simulations. *J. Phys. Chem. C* **2014**, *118*, 23599-23604.
- (26) Finotello, A.; Bara, J. E.; Camper, D.; Noble, R. D. Room-temperature ionic liquids: Temperature dependence of gas solubility selectivity. *Ind. Eng. Chem. Res.* **2008**, *47*, 3453-3459.
- (27) Turner, C. H.; Cooper, A.; Zhang, Z.; Shannon, M. S.; Bara, J. E. Molecular simulation of the thermophysical properties of N-functionalized alkylimidazoles. *J. Phys. Chem. B* **2012**, *116*, 6529-6535.
- (28) Babarao, R.; Dai, S.; Jiang, D. E. Understanding the high solubility of CO₂ in an ionic liquid with the tetracyanoborate anion. *J. Phys. Chem. B* **2011**, *115*, 9789-9794.
- (29) Kerle, D.; Namayandeh Jorabchi, M.; Ludwig, R.; Wohlrab, S.; Paschek, D. A simple guiding principle for the temperature dependence of the solubility of light gases in imidazolium-based ionic liquids derived from molecular simulations. *Phys. Chem. Chem. Phys.* **2017**, *19*, 1770-1780.
- (30) Tomé, L. C.; Gouveia, A. S. L.; Ab Ranii, M. A.; Lickiss, P. D.; Welton, T.; Marrucho, I. M. Study on Gas Permeation and CO₂ Separation through Ionic Liquid-Based Membranes with Siloxane-Functionalized Cations. *Ind. Eng. Chem. Res.* **2017**, *56*, 2229-2239.
- (31) Carlisle, T. K.; Wiesenauer, E. F.; Nicodemus, G. D.; Gin, D. L.; Noble, R. D. Ideal CO₂/Light Gas Separation Performance of Poly(vinylimidazolium) Membranes and Poly(vinylimidazolium)-Ionic Liquid Composite Films. *Ind. Eng. Chem. Res.* **2013**, *52*, 1023-1032.
- (32) Mittenthal, M. S.; Flowers, B. S.; Bara, J. E.; Whitley, J. W.; Spear, S. K.; Roveda, J. D.; Wallace, D. A.; Shannon, M. S.; Holler, R.; Martens, R.; Daly, D. T. Ionic Polyimides: Hybrid Polymer Architectures and Composites with Ionic Liquids for Advanced Gas Separation Membranes. *Ind. Eng. Chem. Res.* **2017**, *56*, 5055-5069.
- (33) Kupgan, G.; Liyana-Arachchi, T. P.; Colina, C. M. Pore size tuning of poly(styrene-co-vinylbenzyl chloride-co-divinylbenzene) hypercrosslinked polymers: Insights from molecular simulations. *Polymer* **2016**, *99*, 173-184.
- (34) Larsen, G. S.; Lin, P.; Hart, K. E.; Colina, C. M. Molecular Simulations of PIM-1-like Polymers of Intrinsic Microporosity. *Macromolecules* **2011**, *44*, 6944-6951.

- (35) Tian, Z.; Mahurin, S. M.; Dai, S.; Jiang, D. E. Ion-Gated Gas Separation through Porous Graphene. *Nano Lett.* **2017**, *17*, 1802-1807.
- (36) Vicent-Luna, J. M.; Luna-Triguero, A.; Calero, S. Storage and Separation of Carbon Dioxide and Methane in Hydrated Covalent Organic Frameworks. *J. Phys. Chem. C* **2016**, *120*, 23756-23762.
- (37) Raeissi, S.; Peters, C. J. Carbon Dioxide Solubility in the Homologous 1-Alkyl-3-methylimidazolium Bis(trifluoromethylsulfonyl)imide Family. *J. Chem. Eng. Data* **2009**, *54*, 382-386.
- (38) Carvalho, P. J.; Álvarez, V. H.; Marrucho, I. M.; Aznar, M.; Coutinho, J. A. P. High pressure phase behavior of carbon dioxide in 1-butyl-3-methylimidazolium bis(trifluoromethylsulfonyl)imide and 1-butyl-3-methylimidazolium dicyanamide ionic liquids. *J. Supercrit. Fluids* **2009**, *50*, 105-111.
- (39) Aki, S. N. V. K.; Mellein, B. R.; Saurer, E. M.; Brennecke, J. F. High-pressure phase behavior of carbon dioxide with imidazolium-based ionic liquids. *J. Phys. Chem. B* **2004**, *108*, 20355-20365.
- (40) Carvalho, P. J.; Coutinho, J. o. A. P. On the Nonideality of CO₂ Solutions in Ionic Liquids and Other Low Volatile Solvents. *J. Phys. Chem. Lett.* **2010**, *1*, 774-780.
- (41) Singh, R.; Marin-Rimoldi, E.; Maginn, E. J. A Monte Carlo Simulation Study To Predict the Solubility of Carbon Dioxide, Hydrogen, and Their Mixture in the Ionic Liquids 1-Alkyl-3-methylimidazolium bis(trifluoromethanesulfonyl)amide ([C_nmim⁺][Tf₂N⁻],n= 4, 6). *Ind. Eng. Chem. Res.* **2015**, *54*, 4385-4395.
- (42) Becke, A. D. Density-functional thermochemistry. III. The role of exact exchange. *J. Chem. Phys.* **1993**, *98*, 5648-5652.
- (43) Frisch, M. J.; Trucks, G. W.; Schlegel, H. B.; Scuseria, G. E.; Robb, M. A.; Cheeseman, J. R.; Scalmani, G.; Barone, V.; Mennucci, B.; Petersson, G. A.; Nakatsuji, H.; Caricato, M.; Li, X.; Hratchian, H. P.; Izmaylov, A. F.; Bloino, J.; Zheng, G.; Sonnenberg, J. L.; Hada, M.; Ehara, M.; Toyota, K.; Fukuda, R.; Hasegawa, J.; Ishida, M.; Nakajima, T.; Honda, Y.; Kitao, O.; Nakai, H.; Vreven, T.; Montgomery Jr., J. A.; Peralta, J. E.; Ogliaro, F.; Bearpark, M. J.; Heyd, J.; Brothers, E. N.; Kudin, K. N.; Staroverov, V. N.; Kobayashi, R.; Normand, J.; Raghavachari, K.; Rendell, A. P.; Burant, J. C.; Iyengar, S. S.; Tomasi, J.; Cossi, M.; Rega, N.; Millam, N. J.; Klene, M.; Knox, J. E.; Cross, J. B.; Bakken, V.; Adamo, C.; Jaramillo, J.; Gomperts, R.; Stratmann, R. E.; Yazyev, O.; Austin, A. J.; Cammi, R.; Pomelli, C.; Ochterski, J. W.; Martin, R. L.; Morokuma, K.; Zakrzewski, V. G.; Voth, G. A.; Salvador, P.; Dannenberg, J. J.; Dapprich, S.; Daniels, A. D.; Farkas, Ö.; Foresman, J. B.; Ortiz, J. V.; Cioslowski, J.; Fox, D. J.: Gaussian 09. Gaussian, Inc.: Wallingford, CT, USA, 2009.
- (44) Lopes, J. N. C.; Padua, A. A. H. Molecular force field for ionic liquids composed of triflate or bistriflylimide anions. *J. Phys. Chem. B* **2004**, *108*, 16893-16898.

- (45) Lopes, J. N. C.; Deschamps, J.; Padua, A. A. H. Modeling ionic liquids using a systematic all-atom force field. *J. Phys. Chem. B* **2004**, *108*, 2038-2047.
- (46) Aparicio, S.; Alcalde, R.; Davila, M. J.; Garcia, B.; Leal, J. M. Measurements and predictive models for the N-methyl-2-pyrrolidone/water/methanol system. *J. Phys. Chem. B* **2008**, *112*, 11361-11373.
- (47) Potoff, J. J.; Siepmann, J. I. Vapor-liquid equilibria of mixtures containing alkanes, carbon dioxide, and nitrogen. *AIChE J.* **2001**, *47*, 1676-1682.
- (48) Trinh, T. T.; Vlugt, T. J.; Kjelstrup, S. Thermal conductivity of carbon dioxide from non-equilibrium molecular dynamics: a systematic study of several common force fields. *J. Chem. Phys.* **2014**, *141*, 134504-7.
- (49) Martinez, L.; Andrade, R.; Birgin, E. G.; Martinez, J. M. PACKMOL: a package for building initial configurations for molecular dynamics simulations. *J. Comput. Chem.* **2009**, *30*, 2157-2164.
- (50) Van Der Spoel, D.; Lindahl, E.; Hess, B.; Groenhof, G.; Mark, A. E.; Berendsen, H. J. GROMACS: fast, flexible, and free. *J. Comput. Chem.* **2005**, *26*, 1701-1718.
- (51) Essmann, U.; Perera, L.; Berkowitz, M. L.; Darden, T.; Lee, H.; Pedersen, L. G. A smooth particle mesh Ewald method. *J. Chem. Phys.* **1995**, *103*, 8577-8593.
- (52) Hoover, W. G. Canonical dynamics: Equilibrium phase-space distributions. *Phys. Rev. A* **1985**, *31*, 1695-1697.
- (53) Parrinello, M.; Rahman, A. Crystal Structure and Pair Potentials: A Molecular-Dynamics Study. *Phys. Rev. Lett.* **1980**, *45*, 1196-1199.
- (54) Abbott, L. J.; Hart, K. E.; Colina, C. M. Polymatic: a generalized simulated polymerization algorithm for amorphous polymers. *Theor. Chem. Acc.* **2013**, *132*, *1334/1-1334/19*.
- (55) Karayiannis, N. C.; Mavrantzas, V. G.; Theodorou, D. N. Detailed atomistic simulation of the segmental dynamics and barrier properties of amorphous poly(ethylene terephthalate) and poly(ethylene isophthalate). *Macromolecules* **2004**, *37*, 2978-2995.
- (56) Theodorou, D. N.; Suter, U. W. Detailed Molecular-Structure of a Vinyl Polymer Glass. *Macromolecules* **1985**, *18*, 1467-1478.
- (57) Shah, J. K.; Maginn, E. J. A general and efficient Monte Carlo method for sampling intramolecular degrees of freedom of branched and cyclic molecules. *J. Chem. Phys.* **2011**, *135*, 134121-11.
- (58) Gelb, L. D.; Gubbins, K. E. Pore size distributions in porous glasses: A computer simulation study. *Langmuir* **1999**, *15*, 305-308.

- (59) Raeissi, S.; Peters, C. J. High pressure phase behaviour of methane in 1-butyl-3-methylimidazolium bis(trifluoromethylsulfonyl)imide. *Fluid Phase Equilib.* **2010**, 294, 67-71.
- (60) Liu, H.; Zhang, Z.; Bara, J. E.; Turner, C. H. Electrostatic potential within the free volume space of imidazole-based solvents: insights into gas absorption selectivity. *J. Phys. Chem. B* **2014**, *118*, 255-264.

TOC Graphic

